Modelling Solar Powered UAV-BS for 5G and Beyond

(Article begins on next page)

27 April 2024

Modelling Solar Powered UAV-BS for 5G and Beyond

Greta Vallero and Michela Meo
Politecnico di Torino, Italy

Abstract—**Unmanned Aerial Vehicles equipped with Base Stations (UAV-BSs) are considered an effective solution to dynamically provide additional capacity in Radio Access Networks (RANs), in case of network congestion or emergency situations. To face the problem of the poor energy availability provided by on-board batteries, UAV-BSs can be equipped with Photovoltaic (PV) panels. To investigate and understand the complex interworking between traffic needs and energy availability, in this paper, we propose a model of a PV-panel-powered Long Term Evolution (LTE) Multi User Multiple Input-Multiple Output (MU-MIMO) UAV-BS, using a discretized representation of the energy in terms of Energy Packets (EPs). The model highlights the different operation regions under which the traffic demand can be satisfied for given energy production levels. Results for winter and summer seasons that take into account daily traffic and energy production variability are shown and can be used to properly dimension the UAV-BS power supply system.**

Index Terms—**UAV-BS, PV Panel, Queuing Systems, Energy Packets**

I. INTRODUCTION

Mounting a Base Station (BS) on Unmanned Aerial Vehicles (UAVs) have been proposed as a promising solution to dynamically deploy fast and flexible communication facilities, where traditional ground infrastructures are not feasible or cost-effective [1]. Through the additional capacity provided by UAV-BSs, connectivity is brought to the users that are suffering from low-quality of service: UAV-BSs adapt their aerial position where needed, based on position and traffic requirements of users, who are connected to the UAV-BSs through access links, while UAV-BSs are connected to the Core Network (CN), establishing Backhaul (BH) links between them and an Access point (AP). In 5G and beyond 5G systems, the access networks supported by UAV-BSs have been considered for the cases of terrestrial network failures due to network overloads or physical unavailability, like festivals, concerts, sports matches and natural disasters [2]. As introduced in [3], in 6G networks, UAV wireless networks, also known as UAV-assisted networks, or drone cells, beside being employed to provide additional radio coverage, will be also used as content providers and computing servers, in order to meet the growing traffic demand, which is expected to reach 1 zettabyte per month in 2028 and might saturate the 5G capacity within 2030 [3], [4].

The new role of the UAVs in the RANs is possible because of the advance of their structure, which makes most recent drones able to carry up heavy payloads. Up to some years ago, no more than 600 g payload could be brought, while the most recent drones can transport up to 8 kg, much more than the 2 kg weight needed to bring access and BH network equipment [5]. Nevertheless, an important challenge that needs to be addressed is related to the scarce on-board energy availability that is provided to UAV-BSs by on-board batteries. This is an issue which actually characterises UAVs in general but, when they are used as communication infrastructure, the situation worsens. Indeed, besides the energy needed for the flight of the UAV, also the communication unit has to be powered to provide the service [2], resulting in an higher energy consumption and reduction of the UAV-BS lifetime. To cope with this, solar-powered UAV-BSs have been proposed, which result in a longer UAV-BS survival, without adding significant mass to the device [6], [7]. While the solution is promising, several issues need to be tackled. In [8]–[10], the optimal UAV-BSs location is optimised, revealing that a higher UAV-BSs altitude increases the PV panel production, while negatively affecting the Quality of Service (QoS). The survey in [2] highlights that the solar panel dimensioning and the understanding of the effect of intermittent energy production on the communication service provided by UAV-BSs network is usually neglected in literature.

In this paper, we study the dimensioning of the PV power supply system of the LTE MU-MIMO UAV-BS by investigating the interplay between traffic demand and energy generation. To avoid that the energy consumption of the communication unit negatively affects the lifetime of the UAV, we assume that the amount of needed energy is provided by the PV panel, while the power for the UAV-BS flight is taken from the battery. Without loss of generality, we consider these two energy consuming entities as independent and we leave the effects of their possible power exchange as future work. We model the communication unit supply as a queuing system using a discretized representation of data and energy flows, as Data Packets (DPs) and Energy Packets (EPs), as in [11], [12]. The transmission of a DP is triggered by the arrival of an EP. When an EP reaches the system, but no DPs are available or the system is already processing a DP, that EP is unused and, if enough battery capacity is available, moved to the battery and employed to power the UAV-BS flight. Through the queue stability conditions, we investigate the energy production levels that are needed to satisfy the traffic demand. The probability that an EP is unused is derived, and the trade-off between the system stability and energy losses is discussed. Finally, the time variation of both the produced energy and traffic demand is considered to make the system more realistic and to

derive the proper dimension of the PV panel which should be installed on the UAV.

II. RELATED WORK

To exploit the potential of the UAV-BSs networks, a key challenge to address is the scarce on-board energy availability [13]–[15]. Indeed, typically, UAV-BSs are powered by on-board batteries, which limit the survival of these drones. To overcome this, solar-powered UAV-BSs have been proposed in literature: in many studies, they are equipped with PV panels to produce electricity, without adding significant mass or size [2]. Authors in [6] prototype a solar-powered drone, which can fly for 28 hours, while in [8], Sun et al. maximise the system throughput of a UAV-BSs network, powered by PV panels, which are installed on each drone. Besides this, the usage of the solar energy for the network infrastructures supply, and for the BSs of RANs in particular, has been receiving a lot of attention for many years since its usage allows to make the networks more self-sustainable, energy efficient, reducing also the electricity bill [16]. Also the modelling community focuses on the dynamics of the renewable energy harvesting in communication systems, to derive its formal representation, which is fundamental for its proper design, dimensioning and quantification of the effects of the changes of its components to satisfy the needed requirements. These works typically use a discretized representation of data flow, digitalized in DPs, as well as of energy, in terms of EPs, which correspond to the amount of energy which is needed to process a DP [12]. Authors in [17] provides the Markov model of a BS totally powered by renewable energy sources. The model consists of a three-queue system: the first acts as an energy storage, the second is the data queue and the third is used as a reserve energy queue. An analytical model for a generic energy harvesting transmitter, equipped with an energy battery, where incoming EPs are stored, is presented in [18], which formulates the outage and the overflow probabilities due to lack of energy and the throughput.

III. SYSTEM DESCRIPTION

The considered scenario is depicted in Fig. 1. The UAV-BS provides additional capacity to users, who access the CN using the access links, between users and the UAV-BS, and the BH links, which are established between the UAV and an AP. As in [19], we consider a femto cell BS, equipped with multiple antennas, using the Multi-User Multiple Input-Multiple Output (MU-MIMO). The access network uses a 2.6 GHz LTE femto cell based technology, whose link budget is set as in [20], according to which the radio coverage is 830 m, in Line-of-Sight. The BH links work on the 3.5 GHz frequency and bandwidth of 20 MHz, consisting of 100 Resource Blocks (RBs) [21]–[23]. The UAV-BS is equipped with a PV panel that harvests energy from solar and converts it to electrical energy. The PV panel is used to supply the transmitting unit of the drone, while the battery is used to make the drone fly. In this work we focus on the PV panel which produces energy for data transmission.
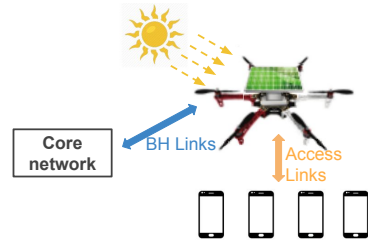

Fig. 1. Solar-powered UAV communication system, where the UAV-BS is equipped with solar panels that harvest energy from solar source.
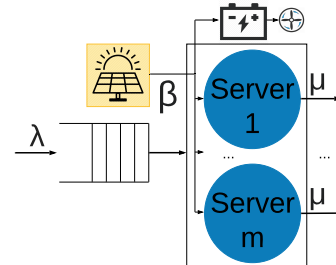

Fig. 2. Model of the considered system.

The MU-MIMO femtocell BS is modelled as a queuing system with m servers, as depicted in Fig. 2, where each server represents a single MIMO antenna. Data and energy flows are discretized in DPs and EPs, respectively, and the waiting line in which the DPs are waiting to be transmitted is assumed to be infinite. To transmit a DP, a server needs an EP. This means that as soon as the server ends the transmission of a DP, it switches to sleep mode until an EP arrives. When this occurs, if there is at least a DP in the DP waiting line and an available server, the server is activated and a new transmission starts. In case there is no DPs to be transmitted, that EP is considered lost and can not be used for the transmission of a DP. An EP that reaches the system while all the servers are busy, sending DPs, is lost, as well. As already mentioned and illustrated in Fig. 2, actually the lost EPs are not wasted, but moved and stored in the energy battery, if enough capacity is available, and employed to supply the UAV-BS mobility. As in [24], [25], DPs and EPs arrive at the system according to Poisson processes with rate λ and β, respectively; the DP transmission time has an exponential distribution with parameter μ.

IV. MODEL DESCRIPTION AND ANALYSIS

A. Analysis of the single server DP queue

We start by analysing the LTE BS equipped with a single MIMO antenna. This is modelled as a single server queuing system, as reported in Fig. 2. As described before, when the server completes a service, it switches to sleep mode, until an EP arrives; when an EP arrives, if there is a DP in the data queue, a new transmission starts. The system is equivalent to the one drawn in Fig. 3: when the server finishes a DP transmission, it enters into a vacation time, during which it is inactive and waiting for the next EP arrival. This is modelled as a *sleeping box* (represented in green in Fig. 3), acting as a delayer, before the server can start transmitting the next DP in the queue, if any. The time
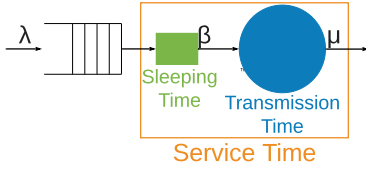
Fig. 3. Model for the single server DP queue.

spent in the sleeping box is exponentially distributed, with parameter β and we call it *sleeping time*. Once this time expires, i.e., an EP arrives, the server is reactivated and, if there is a DP in the waiting line, the actual transmission starts (see blue part in Fig. 3) and lasts for the *transmission time*. The *service time* is defined as the time a DP spends in the orange rectangle in Fig. 3. It is given by the sum of the sleeping time (that is the time waiting for the EP) and the transmission time. In our case, this is given by the sum of two exponential random variables with parameters β and μ, respectively. The system can then be modelled as an M/G/1 queue, where the probability density function of the service time G, as discussed in [26], is $f_G(x) = (\beta\mu)/(\beta-\mu)(e^{-\mu x} - e^{-\beta x})$.
The mean value of the service time, $E[G]$, and the variance $Var[G]$ are, respectively, $\frac{1}{\beta} + \frac{1}{\mu}$ and $\frac{\beta^2 + \mu^2}{\beta^2 \mu^2}$. The M/G/1 queue is stable if $\lambda E[G] < 1$, that is $\lambda < \frac{1}{E[G]}$; hence, the system is stable if:

$$\lambda < \frac{\beta\mu}{\beta + \mu} \tag{1}$$

Probability that an EP is lost: The probability that an EP is lost, L_{EP}, can be written as $L_{EP} = L_{EP,empty} + L_{EP,busy}$, where $L_{EP,empty}$ is the probability that an EP is lost because when it arrives no DPs are present in the system, the server remains in sleep mode and no transmission starts; it is given by the probability to find the queuing system empty:

$$L_{EP,empty} = 1 - \lambda E[G] \tag{2}$$

$L_{EP,busy}$ is the probability that the EP is discarded since, when it reaches the system, the server is active and transmitting a DP:

$$L_{EP,busy} = \lambda E[G] \frac{1/\mu}{1/\mu + 1/\beta} = \frac{\lambda}{\mu} \tag{3}$$

which is the probability that the queue is not empty ($\lambda E[G]$) multiplied by the probability that the server is processing instead of sleeping.
Out of the stability condition, which means that (1) is not satisfied, $L_{EP,empty}$ is zero, since the DP queue diverges and there are always DPs waiting to be transmitted. Similarly, since there is always some DPs waiting in the queue, transmission times alternate with times waiting an EP to arrive, and an EP is lost if it arrives during a transmission time. The probability that an EP is lost is $L_{EP,busy} = \frac{1/\mu}{1/\mu + 1/\beta} = \frac{\beta}{\mu+\beta}$.

B. Analysis of the DP queue with multiple servers

We now discuss the LTE BS, equipped with multiple MIMO antennas, using MU-MIMO. This is modelled

as a multiple servers system, each server representing a single MIMO antenna. The system can be modelled as a bidimensional Continuous-Time Markov Chain (CTMC) $X = \{X(t)\}$ in which the state is given by $\overline{s} = (d, p)$, where d is the number of DPs in the system (both waiting and being transmitted) and p is the number of servers that are transmitting a DP, i.e., the number of transmitting MIMO antennas. Transitions are reported in Table I. Arrivals occur with rate λ and increase by one the number of DPs in the system, d. A departure of a DP occurs with rate $p\mu$, where μ is the service rate and p is the number of servers that are transmitting a DP. Finally, a transmission starts if there are available servers ($p < m$), some DPs that are waiting ($d > p$) and an EP arrives with rate β.
To study the ergodicity of the system let us focus on the *service capacity* of the system with m servers, or the *maximum service rate* that the system can reach. The maximum service rate is reached when the load is high and there are always DPs to transmit. To investigate this situation, we introduce a new model that we call *maximum service rate model*. The model is an M/M/m/m queue in which services represent DPs transmission, and the customers represent the EPs that enable a service to start: as soon as an EP arrives, a transmission can start if some server is available. Since the EPs cannot be stored, the capacity of the waiting line is zero. The probability to lose an EP in these conditions is denoted by $L^*_{EP,busy}$ and is given by the probability that an EP arrives and finds all the m servers already busy. This probability is the loss probability of the M/M/m/m queue, the very well-known Erlang-B formula, $E_B(m, \beta/\mu)$:

$$L^*_{EP,busy} = E_B(m, \beta/\mu) = \frac{1/m!(\beta/\mu)^m}{\sum_{i=0}^{m} 1/i!(\beta/\mu)^i} \tag{4}$$

The throughput of the service capacity model, which represents the maximum service rate of the DP queue with multiple servers, is equal to:

$$S_M = \beta \left(1 - L^*_{EP,busy}\right) \tag{5}$$

Hence, the DP queue with multiple servers is stable and the CTMC X is ergodic and reaches a steady-state distribution if the DP arrival rate is smaller than the maximum service rate, i.e., if the following condition holds:

$$\lambda < \beta \left(1 - L^*_{EP,busy}\right) \tag{6}$$

From the solution of the CTMC X under the ergodicity condition, it is possible to derive the performance indicators when the system is stable. Let $\pi(d, p)$ be the steady-state probability to have d DPs in the system and p servers that are processing DPs. We can derive the probability that an EP is lost because it finds no DP that needs to be processed:

$$L_{EP,empty} = \sum_{p=0}^{m-1} \pi(p, p)$$

TABLE I
TRANSITIONS OUT OF STATE $\overline{s} = (d, p)$

Destination state	rate
$(d + 1, p)$	λ
$(d - 1, p - 1)$ for $p > 0$	$p\mu$
$(d, p + 1)$ for $p < m \wedge d > p$	β

and the probability that an EP is lost because when it arrives at the system all the servers are already busy processing DPs:

$$L_{EP,busy} = \sum_{d=m}^{\infty} \pi(d, m)$$

V. LOSS PROBABILITY

In this section, the models previously discussed are verified by simulation experiments. We simulate our scenario with $m = 1, 2, 3, 4$ servers, β and μ equal to 0.5 and 1.0, respectively, and λ varying between 0.1 and 0.89, with granularity 0.01. We measure the EP loss probability, which is the probability to lose an EP. Remind that lost EPs are actually not wasted, but moved to the battery and used for the supply of the UAV-BS flight. Fig. 4 reports the total probability of losing an EP, L_{EP} (on the left), the probability to lose an EP because there are no DPs to serve, $L_{EP,empty}$ (in the middle), and the probability to lose it because the servers are busy, $L_{EP,busy}$ (on the right). Loss probabilities are shown versus λ and the cases with $m = 1, 2, 3, 4$ servers are plotted, respectively, in blue, orange, green and red. Vertical lines show the ergodicity condition on λ as in (6), while the horizontal dashed lines in the plot on the left indicate $L_{EP,busy}^*$ as in (4).

Observe the two different regions which correspond to the queue being stable or not and that differ for the behaviour of the loss probabilities. For low values of λ, the DP queue is stable. As λ grows the probability to lose an EP because it finds the queue empty ($L_{EP,empty}$) decreases while it becomes the more and more likely that the EP finds the server(s) busy ($L_{EP,busy}$ grows). Interestingly, when the system is stable, L_{EP} assumes the same values, independently on the number of servers. When the number of servers grows, the probability to lose EPs because the servers are all busy is smaller but this is compensated by the probability to lose and EP because the queue is empty. When the queue becomes unstable, i.e, when λ exceeds the condition in (6), the probability $L_{EP,empty}$ is zero, while the probability $L_{EP,busy}$ is given by $L_{EP,busy}^*$, as in (4).

Let us now focus on the ergodicity condition. While increasing the number of servers from 1 to 2 has an important beneficial effect on the maximum service rate, any additional server produces only marginal improvements, which tend to vanish. Indeed, by increasing the number of servers, the probability $L_{EP,busy}^*$ reduces and reaches zero, but the maximum service rate in (5) converges to the EP arrival rate β. Hence, we can conclude that by increasing the number of servers, it is possible to increase the maximum service rate (less tight ergodicity condition) but no benefits are achieved in terms of EP loss probability.

However, the benefits of additional servers can be observed only as far as their aggregate transmission capacity is small; when the transmission capacity is large enough, the system is constrained by the energy production system. In order to further increase the system service capacity, a more powerful energy production system is needed.

VI. DIMENSIONING UAV-BSs

A. EP and DP Rates Models

In order to properly model the size of the PV panel which is installed on each UAV-BS, we consider the hourly fluctuation of the energy production and of the data traffic. Hence, the EP and DP rates are not constant but time dependant and denoted by $\beta(t)$ and $\lambda(t)$, respectively. To model the hourly variation of the rates, we start from real PV panel energy production data; and we take data provided by PV-WATT [27]. The data estimates the electricity production of a typical poly- or mono-crystalline silicon PV-panel system, taking into consideration realistic solar irradiation patterns, corresponding to the typical meteorological year in the considered area, with a granularity of one hour. The main typical losses occurring in a real PV panel system during the process of solar radiation conversion into electricity are accounted for 14%. The efficiency achieves 20% [28], which means that about $5 \ m^2$ can be assumed per each kWp of PV panel capacity [29], while its weight is 2.55 kg per m^2, for off-the-shelf portable PV panels. The elevation at which the PV panel operates, if it is installed on an UAV-BS, makes it more efficient, since it is working at lower temperature and this increases the energy production between 7% and 12%, as reported in [30]. For this reason, the data of energy production provided by PV-WATT are increased by 7%. We normalise the hourly energy generation during the year, so that the generated energy in each hour is given as a fraction of the yearly peak hour production. Then, the meteorological winter and summer periods are selected, using the normalised energy production from 1st December to 28th February and from 1st June to 31st August, respectively. The average hourly energy production during the day is computed, which provides the shape of the hourly EP arrival rate during the typical day in the winter and summer seasons, which are reported in Fig. 5, in blue and orange, respectively. Thus, the hourly EP arrival rate, in EP/s, is derived as:

$$\beta(t) = B \cdot f_n^{(E)}(t) \tag{7}$$

where $f_n^{(E)}(t)$ is the energy production shape as previously derived and B, in EP/s, is the factor which defines the arrival rate of EPs.

To formalise the variation of the traffic demand, we use the traffic data provided by a large Italian Mobile Network Operator, which report the traffic demand volume, in bits, in a wide area around Milan, in Italy, for a duration of two months in 2015, with granularity of 15 minutes. Data are aggregated to have an hourly granularity and the average hourly traffic demand during the day is computed. Then, data are normalised and the daily pattern $f_n^{(D)}(t)$ is
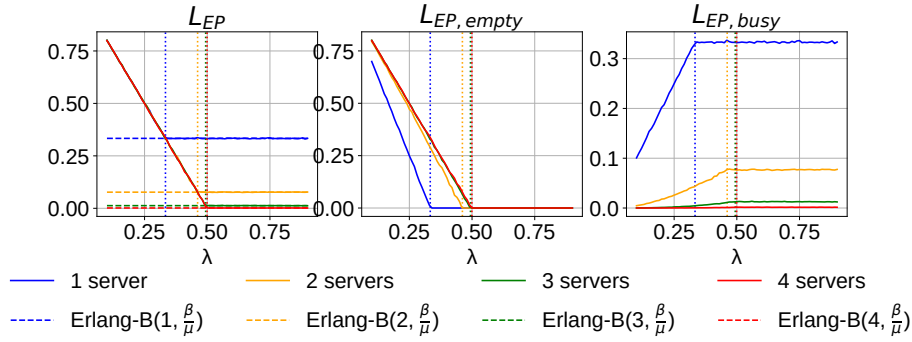
Fig. 4. L_{EP} (on the left), $L_{EP,Busy}$ (in the middle) and $L_{EP,Empty}$ (on the right), versus λ and with different number of servers. Vertical lines represent stability conditions, dashed horizontal lines report the EP loss probability given by the Erlang-B formula in (4).
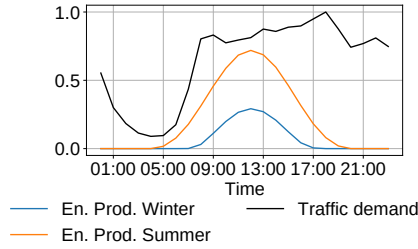

Fig. 5. Normalised pattern for the hourly traffic demand (in black) and for the hourly energy production in winter (in blue) and in summer (in orange).

obtained; it is reported in black in Fig. 5. The parameter $\lambda(t)$, in DP/s, is computed as follows:

$$\lambda(t) = L \cdot f_n^{(D)}(t) \qquad (8)$$

where L, in DP/s, is a factor, which scales the amplitude traffic rate.

B. Model of the PV Panel

We now derive the size of the PV panel which has to be installed on each UAV-BS to make the system stable; i.e., to serve the traffic. The parameter B, in EP/s, is defined as:

$$B = \frac{C_{PV}}{EP_j} R_{peak} \qquad (9)$$

where C_{PV} is the capacity of the PV-panel in watt, EP_j is the energy carried by an EP, in J/EP, and R_{peak} is the ratio between the yearly maximum power production per hour of the considered PV-panel and its nominal capacity and it varies according to the location of the PV-panel. Substituting (9) in (1), the system results stable if the following condition holds:

$$\frac{\lambda(t) \cdot \mu}{\mu - \lambda(t)} \frac{EP_j}{R_{peak} f_n^{(E)}(t)} < C_{PV} \qquad (10)$$

C. Parameters Setting

In this part of the work, we consider a LTE MU-MIMO UAV-BS, equipped with a single MIMO antenna, which supports the ground RAN providing additional capacity to users. We assume that its bit rate BR is the weighted average of the access and BH bit rate, BR_A and BR_{BH},

TABLE II
PARAMETERS SETTING

$Elevation$ [m]	P_A [W]	P_{BH} [W]	EP_j [mJ]
70	17	79.96	6
120	15.89	93.04	6.33

TABLE III
SUMMARY OF PV PANEL CAPACITY, SURFACE AND WEIGHT

B	C_{PV} [W]		$Surface$ [m]		$Weight$ [kg]	
	70 m	120 m	70 m	120 m	70 m	120 m
0.1	0.7	0.83	0.04	0.04	0.1	0.1
3	23.68	24.98	0.1	0.1	0.25	0.25
5	39.47	41.64	0.19	0.2	0.48	0.51
7	55.26	58.29	0.28	0.29	0.71	0.74
10	78.95	83.27	0.39	0.41	0.99	1.04

computed as $(BR_A \cdot T_A + BR_{BH} \cdot T_{BH})/(T_A + T_{BH})$, where T_A and T_{BH} are the time needed to transmit a DP in the access and BH networks, respectively. BR_A and BR_{BH}, taken from [20], are 16.9 Mbit/s and 72 Mbit/s, respectively, while T_A and T_{BH} are, respectively, equal to $3.35 \cdot 10^{-4}$ s and $0.79 \cdot 10^{-4}$ s, assuming that the size of each DP is 709 bytes, as in [31]. From these parameters, we derive that BR is 27.38 Mbit/s and μ is 4.28 DP/ms. The size of each EP, which is the necessary amount of energy needed to transmit a DP, is the average between the energy needed for the transmission of a DP in the access and in the BH network. To compute these values, the models employed in [20], [32], [33] are used, which depend on the hardware components of the antenna, as well as on the transmitted power, which varies with the elevation of the drone. Here, we assume two different elevations, set equal to 70 m and 120 m, since the maximum allowed drone elevation until 31st December 2020, in Italy, is 70 m but from 1st January 2021 considered drones are allowed to fly up to 120 m, according to the European regulation reported in [34]. Given the power consumption of the access and the BH interfaces, P_A and P_{BH}, respectively, taken from [33] and reported in Table II, at the two considered elevations, the size of each EP, EP_j, in joule, is $EP_j = 0.5 \cdot (P_A \cdot T_A + P_{BH} \cdot T_{BH})$, where T_A and T_{BH} denote the time needed to transmit a DP in the access and BH network, respectively. Because of the difference of P_A and P_{BH} at
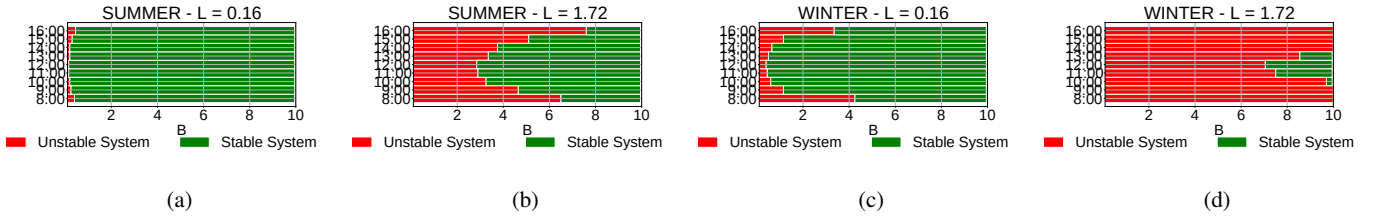
Fig. 6. Values of B which make the system stable (enough energy for traffic demand) during each hour under high traffic ($L = 1.72$) and low traffic ($L = 1.72$), in summer (a) and (b) and in winter (c) and (d).
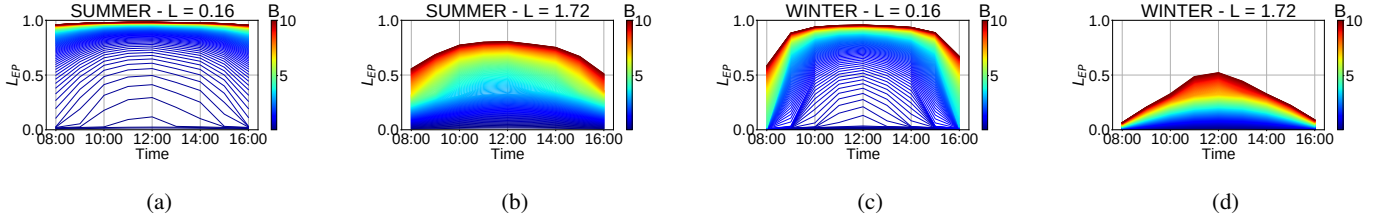

Fig. 7. Hourly L_{EP} in summer with $L = 0.16$ (a) and $L = 1.72$ (b) and winter with $L = 0.16$ (c) and $L = 1.72$ (d).

the two different elevations, the EP size is larger if the drone is at 120 m than when it operates at 70 m (see Table II), since more power is transmitted to reach the users. Finally, from solar production data provided by [27], we know that the yearly maximum power production of a PV panel installed in Turin, is equal to 76% of its nominal capacity and R_{peak} is set accordingly.

D. Performance evaluation

Through the stability of the system, we investigate the capability of the UAV-BS to serve the traffic demand and the relation between traffic and energy production. We focus on daylight time, i.e. from 8:00 to 17:00. On x-axis of Fig. 6, the parameter B, which determines the energy production as in (7), varies from 0.1 to 10.0. As previously mentioned, the nominal capacity of the PV panel corresponding to a value of B depends on the elevation at which the UAV-BS is operating. When B is 0.1, the nominal capacity of the PV panel is 0.79 W and 0.83 W, if it is 70 m and 120 m, respectively, corresponding to a surface of $0.4 \cdot 10^{-2}$ m^2 and a weight no larger than 0.1 kg; with B equal to 10.0, the nominal capacities are 78.95 W and 83.27 W, which means a PV panel surface of 0.4 m^2, with weight around 1 kg. For the considered elevations, the capacity, surface and weight for different values of B in the considered interval, are reported in Table III. The table indicates that the considered PV panels are small enough, in terms of both surface and weight, to make their installation feasible on a UAV-BS.

The green and red bars in Fig. 6 indicate the values of B, which make the system stable and unstable during each hour reported on the y-axis: when the system is unstable, the energy is not enough to serve all traffic demand. Results are given for two different values of traffic, represented by L equal to 0.16 and 1.72, in Figs. 6b and 6d, in summer and winter. The figure shows that, as expected, low traffic demand can always be satisfied even in winter with limited energy production; while high traffic demand are satisfied

only in summer, when the energy production is high and large PV panels are considered. Larger values of B are needed to serve the traffic during low energy production hours, from 8:00 to 10:00 and from 14:00 to 16:00, than during the peak energy production period, from 11:00 to 13:00.

The probability to lose EPs, L_{EP}, is plotted in Figs. 7, where each curve corresponds to a given hour of the day; different values of B are considered, from 0.1, in blue, to 10.0, in red. L_{EP} grows when lower energy production levels are needed: that is when traffic is low and production is high. Indeed, the peack of L_{EP} always occurs at 12:00. In particular, at 12:00, in summer, B equal to 0.15 and 2.85 stabilises the system, when L is 0.16 and 1.72, respectively, maintaining L_{EP} no larger than 0.02 and 0.32. At 16:00 values of B larger than 0.45 and 7.6 are needed. This means that in summer during peak hours production, if the UAV-BS operates at 120 m of altitude, it needs a PV panel with capacity of 1.2 W and 24 W, while, if it is at 70 m, the capacity slightly decreases to 1.1 W and 22.5 W. For both the elevations, these nominal capacities correspond to a panel surface of $0.6 \cdot 10^{-2}$ m^2 and 0.12 m^2, if L is 0.16 and 1.72, respectively. In case the UAV-BS provides the service out of the peak of the energy production, the needed PV panel capacity at 120 m increases up to 3.7 W and 63 W, corresponding to PV panel areas no larger than 0.02 m^2 and 0.3 m^2. In case the UAV-BS operates at 70 m, the needed nominal capacities are 3.55 W and 60 W, without significant reductions of PV panel surface.

In winter, the situation is similar as illustrated in Figs. 6c, 6d, 7c, 7d, even if larger values of B than in summer are needed and lower values of L_{EP} are reached, because of the low energy production, which characterises this season, as shown in Fig. 5. At 8:00 and 16:00, when L is 0.16, B greater than 4.2 and 3.35, respectively, is needed in order to stabilise the system, keeping L_{EP} lower than 0.03. This means that with this traffic intensity, a PV panel whose
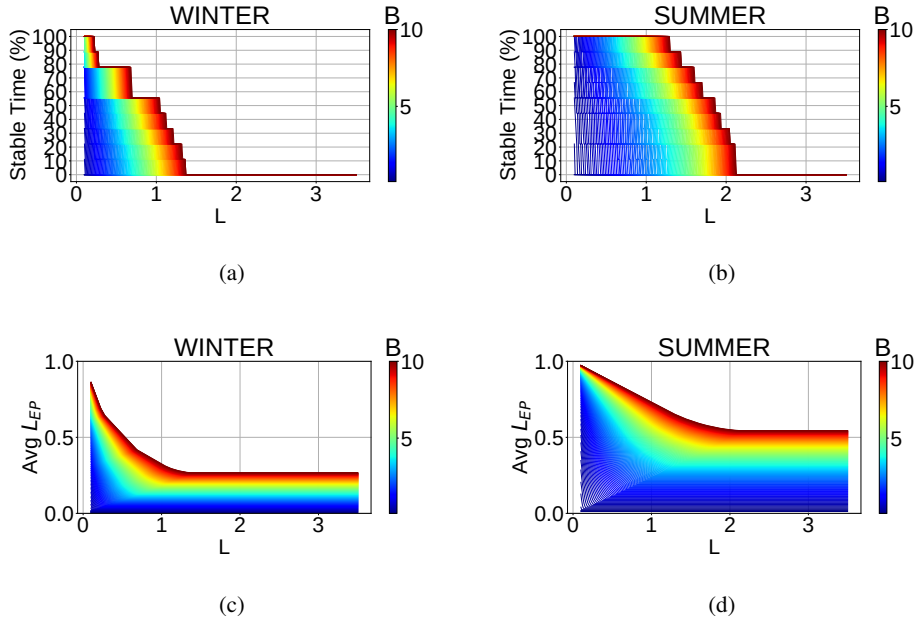
Fig. 8. Percentage of time during which the system is stable in winter (a) and summer (b); Average L_{EP} in winter (c) and summer (d).

nominal capacity is between 28 W and 35 W is needed if the UAV-BS is located at 120 m, which has a surface between 0.17 m^2 and 0.14 m^2. This capacity rises between 26.4 W and 33 W, with no significant variation of the needed PV-panel area, if the UAV-BS elevation is 70 m. At 12:00 B equal to 0.4 is sufficient to make the system stable, provided by a PV panel with nominal capacity of 3.3 W and surface equal to $0.17 \cdot 10^{-1}$ m^2. In these cases, L_{EP} is 0.03. Increasing L up to 1.72, i.e. increasing the traffic intensity, only during the peak hour production, from 10:00 to 14:00, B larger than 7.05 makes the system stable, with L_{EP} no larger than 0.32, which is achieved when the installed PV panel capacity is 71 W, which has a surface of 0.3 m^2.

Separately considering winter and summer, Figs. 8a and 8b provide the percentage of time during a day for which the system is stable increasing the value of L (and, hence, the traffic) from 0.1 to 3.5. Each curve in the figures corresponds to a different value of B, from 0.1, in blue, to 10.0, in red. These figures confirm that large values of L require large values of B to achieve the stability of the system. In winter, the system is stable 100% of the time (meaning it can serve all the traffic at each time of the day) only if traffic is low (L is between 0.1 and 0.22), and the production system is large (B larger than 7.8). The nominal capacity of the PV-panel that is is needed is at least 61.58 W, if the UAB-BS is located at 70 m, while it is at least 64.95 W, when it works 120 m above the ground. If lower values of B are used, the system reaches stability less than 80% of the considered time and with B lower than 1, which corresponds to a nominal capacity smaller than 9 W, for both the considered elevations, instability occurs for more than half of time. In summer, the situation is better and the system is stable for the whole considered time even under high traffic (L up to 1.29), if B is larger than 9.95. The system results stable for more than 80% of the time

when L is 0.43, if B is between 2.0 and 10, i.e. if the nominal capacity of the PV panel is 15.8 W, if the drone height is 70 m, and 16.7 W, if the UAV-BS is located at 120 m above the ground, but for less than 60%, if B is lower than 1.45, which is the scenario where a PV-panel with nominal capacity of 12 W is employed.

As discussed above, large values of B and small values of L, beside making the system stable, generate large values of energy losses L_{EP} as shown in Figs. 8c and 8d. L_{EP} decreases with B and L, until the region where the system is unstable, where L_{EP} assumes a constant value, which is up to 0.54, in summer and up to 0.27, in winter, according to the B and L setting.

These results show how the models proposed in the previous sections can be used to understand the relation between traffic demand and power supply and to dimension the UAV-BS power supply system. Results also highlight the importance of the evaluation of the period of the day and of the year in order to verify the feasibility of this solution and its proper sizing.

VII. Conclusion

The use of UAVs, on which BS equipment is mounted, is a promising solution to dynamically provide additional capacity in RANs. Usually, these UAV-BSs are powered by on-board batteries, which makes their survival short, because of the scarceness of the energy availability. For this reason, solar-powered UAV-BSs are an interesting alternative which, however, raises a number of challenges related to its dimensioning and the intermittent nature of energy generation. In this paper, we model a PV-panel powered LTE MU-MIMO UAV-BS and investigate the different system operation regions, as function of traffic demand and energy production. Our results reveal that the usage of the PV panel as a unique energy source for the communication unit of an UAV-BS is an effective solution

but it has to be properly sized in order to operate in stability conditions.

REFERENCES

[1] Q. Wu *et al.*, "Joint trajectory and communication design for multi-uav enabled wireless networks," *IEEE Transactions on Wireless Communications*, vol. 17, no. 3, pp. 2109–2121, 2018.

[2] B. Li *et al.*, "Uav communications for 5g and beyond: Recent advances and future trends," *IEEE Internet of Things Journal*, vol. 6, no. 2, pp. 2241–2263, 2018.

[3] F. Tariq *et al.*, "A speculative study on 6g," *IEEE Wireless Communications*, vol. 27, no. 4, pp. 118–125, 2020.

[4] F. Khan, "Multi-comm-core architecture for terabit-per-second wireless," *IEEE Communications Magazine*, vol. 54, no. 4, pp. 124–129, 2016.

[5] L. Microsystem. (2015) Lime demonstrates fprf transceivers at mobile world congress shanghai. [Online]. Available: https://limemicro.com/news/limedemonstrate-fprf-transceiversatmobileworldcongressshanghai/

[6] P. Oettershagen *et al.*, "Perpetual flight with a small solar-powered uav: Flight results, performance analysis and model validation," in *2016 IEEE Aerospace Conference*. IEEE, 2016, pp. 1–8.

[7] S. Morton *et al.*, "Solar powered uav: Design and experiments," in *2015 IEEE/RSJ International Conference on Intelligent Robots and Systems (IROS)*. IEEE, 2015, pp. 2460–2466.

[8] Y. Sun *et al.*, "Resource allocation for solar powered uav communication systems," in *2018 IEEE 19th International Workshop on Signal Processing Advances in Wireless Communications (SPAWC)*. IEEE, 2018, pp. 1–5.

[9] J. Wu *et al.*, "Path planning for solar-powered uav in urban environment," *Neurocomputing*, vol. 275, pp. 2055–2065, 2018.

[10] Y. Sun *et al.*, "Optimal 3d-trajectory design and resource allocation for solar-powered uav communication systems," *IEEE Transactions on Communications*, vol. 67, no. 6, pp. 4281–4298, 2019.

[11] E. Gelenbe, "Energy packet networks: Ict based energy allocation and storage," in *International Conference on Green Communications and Networking*. Springer, 2011, pp. 186–195.

[12] E. Gelenbe *et al.*, "An energy packet network model for mobile networks with energy harvesting," *Nonlinear Theory and Its Applications, IEICE*, vol. 9, no. 3, pp. 322–336, 2018.

[13] M. Mozaffari *et al.*, "Efficient deployment of multiple unmanned aerial vehicles for optimal wireless coverage," *IEEE Communications Letters*, vol. 20, no. 8, pp. 1647–1650, 2016.

[14] A. Colpaert *et al.*, "Aerial coverage analysis of cellular systems at lte and mmwave frequencies using 3d city models," *Sensors*, vol. 18, no. 12, p. 4311, 2018.

[15] S. De Bast *et al.*, "Cellular coverage-aware path planning for uavs," in *2019 IEEE 20th International Workshop on Signal Processing Advances in Wireless Communications (SPAWC)*. ieee, 2019, pp. 1–5.

[16] V. Chamola *et al.*, "Solar powered cellular base stations: Current scenario, issues and proposed solutions," *IEEE Communications magazine*, vol. 54, no. 5, pp. 108–114, 2016.

[17] I. Dimitriou *et al.*, "A markovian queueing system for modeling a smart green base station," in *European Workshop on Performance Engineering*. Springer, 2015, pp. 3–18.

[18] S. Akın *et al.*, "On the energy and data storage management in energy harvesting wireless communications," *IEEE Transactions on Communications*, vol. 67, no. 11, pp. 8056–8071, 2019.

[19] A. Adhikary and G. Caire, "On the coexistence of macrocell spatial multiplexing and cognitive femtocells," in *2012 IEEE International Conference on Communications (ICC)*. IEEE, 2012, pp. 6830–6834.

[20] M. Deruyck *et al.*, "Designing uav-aided emergency networks for large-scale disaster scenarios," *EURASIP Journal on Wireless Communications and Networking*, vol. 2018, no. 1, p. 79, 2018.

[21] ETSI, "ETSI TS 136 212 v14.2.0 - LTE; Evolved Universal Terrestrial Radio Access (E-UTRA); Multiplexing and channel coding (3GPP TS 36.212 version 14.2.0 Release 14)," ETSI, Tech. Rep., Apr. 2017.

[22] ——, "ETSI TS 136 101 v14.5.0 - LTE; Evolved Universal Terrestrial Radio Access (E-UTRA); User Equipment (UE) radio transmission and reception (3GPP TS 36.101 version 14.5.0 Release 14)," ETSI, Tech. Rep., Nov. 2017.

[23] ——, "ETSI TS 136 213 v14.6.0 - LTE; Evolved Universal Terrestrial Radio Access (E-UTRA); Physical layer procedures (3GPP TS 36.213 version 14.6.0 Release 14)," ETSI, Tech. Rep., Apr. 2018.

[24] E. De Cuypere *et al.*, "A queueing model of an energy harvesting sensor node with data buffering," *Telecommunication Systems*, vol. 67, no. 2, pp. 281–295, 2018.

[25] E. Gelenbe, "A sensor node with energy harvesting," *ACM SIGMETRICS Performance Evaluation Review*, vol. 42, no. 2, pp. 37–39, 2014.

[26] P. Oguntunde *et al.*, "On the sum of exponentially distributed random variables: A convolution approach," *European Journal of Statistics and Probability*, vol. 2, no. 1, pp. 1–8, 2014.

[27] A. P. Dobos, "Pvwatts version 5 manual," National Renewable Energy Lab.(NREL), Golden, CO (United States), Tech. Rep., 2014.

[28] S. Hua *et al.*, "Application of valve-regulated lead-acid batteries for storage of solar electricity in stand-alone photovoltaic systems in the northwest areas of china," *Journal of Power Sources*, vol. 158, no. 2, pp. 1178–1185, 2006.

[29] D. Renga *et al.*, "Modeling renewable energy production for base stations power supply," in *2016 IEEE International Conference on Smart Grid Communications (SmartGridComm)*. IEEE, 2016, pp. 716–722.

[30] M. K. Panjwani *et al.*, "Effect of altitude on the efficiency of solar panel," *International Journal of Engineering Research and General Science*, vol. 2, no. 4, 2014.

[31] A. Espinal *et al.*, "Traffic model using a novel sniffer that ensures the user data privacy," in *MATEC Web of Conferences*, vol. 292. EDP Sciences, 2019, p. 03002.

[32] M. Deruyck *et al.*, "Towards a deployment tool for wireless access networks with minimal power consumption," in *2010 IEEE 21st International Symposium on Personal, Indoor and Mobile Radio Communications Workshops*. IEEE, 2010, pp. 295–300.

[33] G. Castellanos *et al.*, "Performance evaluation of direct-link backhaul for uav-aided emergency networks," *Sensors*, vol. 19, no. 15, p. 3342, 2019.

[34] "Commission implementing regulation (eu) 2019/947 of 24 may 2019 on the rules and procedures for the operation of unmanned aircraft," *OL 152*, vol. L 218, pp. 45–71.